Research Square

Preprints are preliminary reports that have not undergone peer review.
They should not be considered conclusive, used to inform clinical practice,
or referenced by the media as validated information.

A receptor and chaperone that influences lung MAIT cell number, function, and lung inflammation

Mitchell Kronenberg

mitch@lji.org

La Jolla Institute for Immunology https://orcid.org/0000-0001-6318-6445

Gabriel Ascui

La Jolla Institute for Immunology https://orcid.org/0000-0001-6837-3194

Eleni Phung

La Jolla Institute for Immunology https://orcid.org/0000-0002-1414-748X

Alba Mendis

La Jolla Institute for Immunology

Cindy Luna

La Jolla Institute for Immunology

Priscilla Gonzalez

La Jolla Institute for Immunology

Kenneth Kim

La Jolla Institute of Immunology https://orcid.org/0000-0002-5993-4575

Sara McArdle

La Jolla Institute for Immunology https://orcid.org/0000-0003-3795-3772

Dominic Haas

Scripps Research Institute

Xiaoyan Wang

La Jolla Institute for Immunology

Jihye Han

La Jolla Institute for Immunology

Shilpi Chandra

La Jolla Institute for Immunology

Ann Canonigo-Balancio

La Jolla Institute for Allergy and Immunology https://orcid.org/0000-0002-6502-0243

Ting-Fang Chou

La Jolla Institute for Immunology

Michael Constantinides

Scripps Research https://orcid.org/0000-0003-4770-7751

Kathleen Caron

University of North Carolina at Chapel Hill https://orcid.org/0000-0002-7033-9232

Article

Keywords:

Posted Date: October 19th, 2026

DOI: https://doi.org/10.21203/rs.3.rs-10632260/v1

License: This work is licensed under a Creative Commons Attribution 4.0 International License.
Read Full License

Additional Declarations: There is **NO** Competing Interest.

Abstract

Innate-like T cells are tissue-resident lymphocytes, but the factors that govern their localization to specific tissues, at steady state or after infections, are not well defined. Mucosal-associated invariant T (MAIT) cells are an innate-like T cell population that is relatively frequent in the lungs of mice and humans. Receptor activity-modifying protein 3 (RAMP3) is a member of a family of three proteins that modulate the expression and function of several GPCRs, including those involved in immune responses. Despite this, the role of RAMP3 in T cell immunity has not been widely explored. We found that *Ramp3*$^{-/-}$ mice had increased lung MAIT cells at steady-state or after infection, while other T cell populations were less affected. *Ramp3*$^{-/-}$ mice had increased surface CXCR6 expression, and RAMP3 overexpression reduced CXCR6. CXCR6 was required for the dramatic increase in lung MAIT cells after infection. These data suggest that RAMP3 negatively regulated CXCR6 and limited lung MAIT cell numbers. This has important consequences, because infected *Ramp3*$^{-/-}$ mice had increased IL-17A-secreting lung MAIT cells, but were more susceptible to pulmonary infection, with reduced bacterial clearance, increased cellular infiltration, and immunopathology. The increase in lung MAIT cells after infection occurred predominantly from cells located in the tissue, but in *Ramp3*$^{-/-}$ mice there was evidence for some recruitment to the lung. We have established that RAMP3 is a negative regulator of excessive lung MAIT cell responses, acting in part through CXCR6.

Summary

Receptor activity-modifying protein 3 (RAMP3), a receptor chaperone influences lung MAIT cell number, function, and lung inflammation. By interacting with GPCRs, including CXCR6, RAMP3 emerges as a regulator of lung innate-like T cell immune responses.

Introduction

MAIT cells are mostly tissue-resident in mice [1], and in humans, they express tissue-homing chemokine receptors [1–3]. In mice, MAIT cells differentiate into IFNg-producing MAIT1 or IL-17-producing MAIT17 cells in the thymus; these subsets are also present in the periphery [4–7]. MAIT17 cells are increased in frequency in the skin, lung, and lymph node, while MAIT1 cells are enriched in the liver, spleen, and intestine. Functional MAIT1 and MAIT17 subsets are less well defined in humans, although there is evidence for increased MAIT17 cells in the human lung, especially in children [8–10]. The factors that promote MAIT cell localization to specific tissues, and the selective localization of MAIT cell functional subsets to certain tissues, are not well characterized. There is evidence, however, for a role for the microbiome [3,11]. Also, chemokine receptor expression may play a role at steady state or during inflammation [3,12]. Furthermore, there is even less evidence for counter-regulation or negative regulators of MAIT cell populations in different tissues.

MAIT cells play an important role in host defense against several pathogens, particularly in barrier tissues such as the lung, gut, and skin [13–15]. This implies that MAIT cell localization and homing to these tissues require intensive regulation, in addition to their expression of tissue-homing receptors [2,12,16–18]. Here, we provide evidence that a receptor activity-modifying protein, RAMP3, influences MAIT cell number, function and host protection, in the mouse lung. Receptor activity modulating proteins (RAMPs) are a family of 3 single-pass membrane-spanning accessory proteins with a short C-terminal intracellular domain [19]. RAMP proteins can alter the trafficking and function of G protein-coupled receptors (GPCRs), and in particular, were first found to be an essential component of the calcitonin receptor-like receptor (CALCRL), even capable of altering its ligand specificity [20]. The biological relevance of RAMP proteins has been explored extensively in studies of cardio-pathologies, angiogenesis, and obesity [19]. For example, RAMP1 has been has a role in calcitonin/calcitonin gene-related peptide (CGRP) signaling and has been proposed as a therapeutic target for migraines (Sabharwal et al. 2018). The CALCRL interaction with RAMP2 is required for signaling by the adrenomedullin 1 peptide hormone [21]. A mutation associated with non-immune hydrops fetalis, an extravascular fluid accumulation in fetal tissues, disrupts the association between the calcitonin receptor-like receptor (CALCRL) and RAMP2. In contrast, RAMP3 is capable of trafficking to the plasma membrane in the absence of a cognate GPCR, and unlike RAMP1 and RAMP2, RAMP3 contains a PDZ-binding motif in its C-terminus that regulates its recycling [22]. A different ligand, Adrenomedullin 2 (AM2) binds to RAMP3-CALCRL heterodimer. Aged *Ramp3*$^{-/-}$ mice display decreased body weight, suggesting an age-dependent induction of RAMP3 for normal metabolism [23]. Furthermore, there is increased *ADM2* and *RAMP3* expression in adipose tissue from obese patients [24], further suggesting a role for AM2 regulating body-weight through its receptor.

Because RAMP proteins interact with many GPCRs [25], it would be surprising if they did not influence immune responses. *Ramp3* is part of the 'lung gene expression signature' of mouse invariant natural killer T (iNKT) cells, compared to their counterparts in spleen, thymus and liver [26], while others have also found *Ramp3* to be part of a tissue residency gene expression signature for conventional CD4^{+} T cells and regulatory T cells [27,28]. Recent reports have highlighted the capacity of RAMP-paired receptors to regulate T cell responses by binding calcitonin gene-related peptide (CGRP) released by peripheral nerve cells (Darragh et al., 2024, Kulalert et al., 2024, Hou et al., 2024). Only one of these studies implicated RAMP3. While these few publications focus on the neuroimmune aspects of CGRP-RAMP proteins in the regulation of T cells, RAMPs have also been shown to interact with many chemokine receptors [22]. Interestingly, one of these chemokine receptors is CXCR6. This receptor has shown to be important for iNKT cell maintenance and homing to the liver [30–32] and skin [33], but also for the long-term retention MAIT cells after infection in the bronchial alveolar lavage of the lung [18]. In this study, we provided evidence for a counter-regulatory mechanism in which RAMP3 exerted a brake on the MAIT cell population in the mouse lung.

Results

Lung MAIT cells have high Ramp3 expression correlated with several Gpcrs

To identify transcripts that might be related to mouse MAIT cell accumulation in specific tissues, we analyzed a previously published single-cell transcriptomic dataset for MAIT cells from lung, spleen, thymus and liver [4]. Aside from differentiating MAIT thymocytes, there were relatively few cell clusters or genes that provided examples of tissue specificity. We observed, however, that the major lung MAIT cell cluster, which contained lung MAIT cells almost exclusively, showed the highest expression of *Ramp3* transcripts (Fig. 1a). There were almost no reads detected in MAIT cells from other tissues. This expression pattern was distinct from other RAMP family proteins. *Ramp1* was expressed by MAIT cells in the thymus, liver, spleen, and lung, and overlapped to a great extent with those that had an MAIT17 gene expression signature [4], which are the majority in C57BL/6 mice. In contrast, *Ramp2* transcripts were not expressed by mouse MAIT cells (**Extended Data** Fig. 1a).

To confirm the initial observation of selectively high expression of *Ramp3* by lung MAIT cells, we analyzed the ImmGEN Consortium database to evaluate expression of *Ramp3* across multiple immune cell types [34]. When querying for αβ T cells, gδ T cells, innate lymphoid cells (ILCs) and myeloid populations, lung MAIT cells had the highest expression of *Ramp3* (Fig. 1b). Relatively high expression of *Ramp3* transcripts also were detected in several other populations, including lung iNKT cells, spleen iNKT cells stimulated with LPS, and ILC2 from the small intestine.

As RAMPs interact with different G protein-coupled receptors (GPCRs), we analyzed whether *Ramp* transcripts correlated with the expression of any GPCR genes. Analyzing the major lung MAIT cell cluster that expressed *Ramp3*, transcripts encoding C-X-C motif chemokine receptor 6 (*Cxcr6*), Leukotriene B4 Receptor 1 (*Ltb4r1*), and Cysteinyl Leukotriene Receptor 1 (*Cysltr1*) showed the strongest positive correlation with *Ramp3* (Fig. 1c). Several GPCR transcripts correlated with *Ramp1*, with *Cxcr6* and *Ccr2* showing the strongest correlations. While this analysis is limited by gene dropout in single-cell RNA-seq analyses, a pattern of potential regulated gene interactions emerged.

Increased lung MAIT cells in Ramp3 mice

Based on our transcriptomic analysis, *we* evaluated lung MAIT cells in 129S6/SvEv background mice with a whole-body deficiency of the *Ramp3* gene by flow cytometry **(Extended Data** Fig. 1b). *Ramp3*$^{-/-}$ mice had striking increases in the frequencies and absolute numbers of lung MAIT cells, but not in two other lung innate-like T cell populations, iNKT cells and γδ T cells (Fig. 1d). Surprisingly, in most experiments, heterozygous *Ramp3*$^{+/-}$ mice showed increased lung MAIT cells similar to *Ramp3*$^{-/-}$ mice. Haploinsufficiency in *Ramp3*$^{+/-}$ mice was observed in various other types of experiments, but not consistently. A possible explanation is that RAMP3 interacts with many GPCRs and may have a limiting concentration compared to GPCRs regulating lung MAIT cells. In *Ramp3*$^{-/-}$ mice, however, there were no differences in lung CD4 and CD8 T cells (**Extended Data** Fig. 1c), or lung myeloid populations, B cells

(**Extended Data** Fig. 1d), NK cells or ILC (**Extended Data** Fig. 1e) compared to both control strains, wild-type and heterozygous *Ramp3*$^{+/-}$ mice. Additionally, innate-like T cell populations in liver and spleen, including MAIT cells, were not increased in *Ramp3*$^{-/-}$ mice (**Extended Data** Fig. 1f). The skin is a mouse tissue with the highest proportion of MAIT cells in some colonies [11], however, there also was no increase in skin MAIT cells from *Ramp3*$^{-/-}$ mice (Fig. 1e).

To evaluate whether the increase in lung MAIT cells in *Ramp3*$^{-/-}$ mice was secondary to changes in thymus differentiation, we analyzed thymocytes. There were no differences in the numbers of MAIT, iNKT, or γδ thymocytes in *Ramp3*$^{-/-}$ mice (Fig. 1f). Because MAIT cells proliferate and are exported from the thymus at different differentiation stages [35], we also analyzed MAIT thymocyte proliferation by flow cytometry for Ki67 expression. There was a trend toward reduced Ki67 staining of MAIT thymocytes from *Ramp3*$^{-/-}$ mice, but this difference did not reach significance (**Extended Data** Fig. 1g).

Considering that these results were obtained in total-body knockout mice, we performed a bone marrow chimera experiment using either *Ramp3*$^{+/+}$ or *Ramp3*$^{-/-}$ T cell-depleted donor cells to reconstitute X-ray irradiated mice. Because of the lack of congenic mice on the 129S strain background, irradiated, congenic Ly5.1 C57BL/6 mice were used as recipients, with residual host MAIT cells serving as an internal control. After 120 days, the lungs, livers, and spleens of these mice were analyzed by flow cytometry. Importantly, host mice had no evident signs of graft-versus-host disease. Nearly all of the lung gδ T cells were derived from the bone marrow donor. Donor cell dominance was less pronounced for the MAIT cell population. Importantly, *Ramp3*$^{-/-}$ donors gave rise to a higher percentage of lung MAIT cells than their wild-type donor counterparts. This effect of RAMP3 deficiency was limited to lung MAIT cells (Fig. 1g). These data suggest that *Ramp3*$^{-/-}$ lung MAIT cells have a selective advantage in populating the lung, at least after many weeks of reconstitution. Furthermore, this effect of *Ramp3*$^{-/-}$ deficiency was due to a hematopoietic cell type, but this does not prove a cell-intrinsic effect of *Ramp3*$^{-/-}$ deficiency on MAIT cells.

Taken together, the data show that the highly tissue-specific increase in lung MAIT cells from *Ramp3*$^{-/-}$ mice correlated with the specific increase in *Ramp3* transcripts in these cells. This suggested that RAMP3 could be a negative regulator specifically of the lung MAIT cell population.

Lung MAIT cells are increased in Ramp3 mice after bacterial exposure

MAIT cells undergo a dramatic population increase and functional changes after Infection with intracellular bacteria that produce 5-OP-RU, when combined with TLR ligands [11,36,37]. To explore if RAMP3 deficiency altered MAIT cell function during pulmonary bacterial infection, we exposed *Ramp3*$^{-/-}$ mice and control mice to *Salmonella enterica Typhimurium* BRD509 vaccine strain (BRD509), as retropharyngeal administration of this bacteria is a reliable model for antigen- or infection-mediated

MAIT cell increases [36]. After 6 days, bacteria-induced MAIT cells population was further increased in *Ramp3*$^{-/-}$ and *Ramp3*$^{+/-}$ mice when compared to wildtype (Fig. 2a-c). The majority of lung MAIT cells expressed IL-7R, PD-1, CXCR6, and CD103. KLRG1 and CD103 mark the antigen-exposed or antigen-adapted MAIT1 and MAIT17 populations, respectively [38]. CD103^{+} MAIT cells were decreased in *Ramp3*$^{-/-}$ mice after infection, indicating decreased expression of the α_E integrin and suggesting a possible effect on lung localization (**Extended Data** Fig. 2a-c). There was no difference in the percentage of KLRG1^{+} MAIT cells.

To test if the enhanced increase in lung MAIT cells in infected *Ramp3*$^{-/-}$ mice was cell intrinsic, we performed adoptive transfer experiments. First, MAIT cell numbers were augmented by BRD509 strain inoculation in the lung. After 6 days, expanded MAIT cells were sorted from the lung. *Ramp3*-deficient MAIT cells (*Ramp3*$^{-/-}$ or *Ramp3*$^{+/-}$) were labeled with CellTrace Violet while wildtype (*Ramp3*$^{+/+}$) MAIT cells were labeled with CFSE. Either a pair of *Ramp3*$^{-/-}$ with *Ramp3*$^{+/+}$ cells or *Ramp3*$^{+/-}$ with *Ramp3*$^{+/+}$ cells were co-transferred into *Ramp3*$^{+/+}$ mice. When analyzed 4 days later, the *Ramp3*$^{-/-}$ MAIT cells were not super-represented in the lung or spleen of these mice (**Extended Data** Fig. 2d-e) for this short-term experiment. We also transferred expanded MAIT cells from either genotype into *Rag1*$^{-/-}$ mice that were challenged with a subsequent pulmonary BRD509 strain infection and analyzed at day 6 (Fig. 2d). As expected because of the infection site, there were many more MAIT cells in the lung than the liver. There also was a trend toward increased lung MAIT cells when the donor MAIT cells were from *Ramp3*$^{-/-}$ mice, although this did not reach statistical significance (Fig. 2e). These data suggested that migration of MAIT cells to the lung and/or their short-term survival was not increased by RAMP3 deficiency, but the absence of RAMP3 in MAIT cells ultimately may allow accumulation of more cells in the lung at steady state (Fig. 1d). Also, by day 6 after infection when the lung MAIT cell population is under antigen stimulation and is greatly increasing, the cell-intrinsic effect of *Ramp3* deficiency is suggested by the trend in this data (Fig. 2c, 2e).

Dynamic changes in number of Ramp3 MAIT cells after infection

We stained lung MAIT cells from infected mice for Ki67 expression, but there was not a significant difference between genotypes (**Extended Data** Fig. 2f). Surprisingly, lung MAIT cells from *Ramp3*$^{-/-}$ and *Ramp3*$^{+/-}$ mice incorporated less BrdU over six days, a probe for DNA replication and cell division (Fig. 2f), despite the increased population size. Ki67 staining provided a more immediate measure of cell replication at day 6, while BrdU incorporation reflected the cumulative effect of cell divisions. The relatively low BrdU incorporation, compared to Ki67 staining, suggested that replicating MAIT cells in the lung died, or, less likely, migrated elsewhere. There were also increased levels of activated Caspase3/7 in MAIT cells in the lungs of *Ramp3*$^{-/-}$ mice compared to either control strain at day 6 day (Fig. 2g). Furthermore, when analyzed at 40 days after infection, lung MAIT cells were more decreased in *Ramp3*$^{-/-}$ mice compared to wild-type mice (Fig. 2h). There was a more than 15-fold decrease in MAIT cell number in the lungs of infected *Ramp3*$^{-/-}$ mice ($2.6x10^5 \pm 4.9x10^3$ at 6dpi to $1.7x10^4 \pm 3.7x10^3$ at

40dpi), compared to a much smaller approximately 2-fold decrease in *Ramp3*$^{+/+}$ control mice ($9.1x10^4 \pm 2.3x10^3$ at 6dpi to $4.0x10^4 \pm 7.5x10^3$ at 40dpi). These dynamic changes suggest that the increased MAIT cell population after infection in *Ramp3*$^{-/-}$ mice was under stress, with a greater increase in cell number early on, that by day 6 may have been transitioning, leading to a decreased number of proliferating cells and increased apoptosis, with a much more pronounced population decrease by day 40.

To test if the accumulation of MAIT cells after infection required homing from draining lymph nodes to the lung [39], we treated infected mice with FTY720, which inhibits lymph node egress by inducing the internalization of Sphingosine 1-phosphate receptors. In wild-type mice, there was no difference in lung MAIT cell number between infected PBS- or FTY720-treated groups (Fig. 2i), suggesting that the increase in lung MAIT cells did not occur in a draining lymph node, but instead occurred in the lung tissue, consistent with prior reports [18,40]. However, the absolute number of lung MAIT cells was reduced in the lungs of FTY720-treated *Ramp3*$^{-/-}$ mice, suggesting that the increased MAIT cells in *Ramp3*$^{-/-}$ mice could be partly explained by enhanced migration from a lymphoid or other tissue to the lung (Fig. 2i). The number of MAIT cells was increased in the draining mediastinal lymph node (medLN) of infected *Ramp3*$^{-/-}$ mice compared to both control strains (Fig. 2j), but after FTY720 treatment, similar numbers of MAIT cells were detected between genotypes. The data indicated that the trafficking of MAIT cells in *Ramp3*$^{-/-}$ mice was altered, and although there could be a migration component to the increased lung MAIT cells in the infected *Ramp3*$^{-/-}$ mice, these cells may not be migrating from the draining lymph node.

Ramp3 MAIT cells have altered function

To assess the function of lung MAIT cells in *Ramp3*$^{-/-}$ mice, we performed intracellular cytokine staining. In mice, most lung MAIT cells have a MAIT17 transcriptome and phenotype, with the capacity to produce IL-17A [4,41]. Consistent with this, after activation by phorbol 12-myristate 1-acetate (PMA) and ionomycin, the majority of lung MAIT cells produced IL-17A and very few produced IFNg. In *Ramp3*$^{-/-}$ mice without previous challenge or infection, there was a decrease in IL-17A-producing lung MAIT cells compared to both *Ramp3*$^{-/-}$ and *Ramp3*$^{+/-}$ mice, but without a significant increase in MAIT cells synthesizing IFNg (**Extended Data** Fig. 3a). Based on these results, we speculate that lung MAIT cells receive peripheral cues in the lung that support the capacity to produce IL-17A, and that the factors or niche required to promote IL-17A may be saturated when the MAIT cell number in lung is increased.

After exposure to *Salmonella*, there was a higher proportion of spontaneous IL-17A-secreting MAIT cells in the lungs of *Ramp3*$^{-/-}$ mice analyzed *ex vivo* (Brefeldin A only), while there was not a *Ramp3*-dependent change in the total capacity of IL-17A-production by the lung MAIT cells after PMA and Ionomycin (Fig. 3a-b), although this capacity was reduced in the *Ramp3*$^{-/-}$ lung MAIT cells at steady-state mice (**Extended Data** Fig. 3a). No differences in spontaneous or induced IFNg-production were

detected, although the small percentage of Granzyme B-expressing lung MAIT cells was further reduced in *Ramp3*$^{-/-}$ mice (**Extended Data** Fig. 3b).

To further analyze the state of lung MAIT cells in *Ramp3*$^{-/-}$ mice, we performed bulk RNA-seq on *Ramp3*$^{-/-}$ and control lung MAIT cells before and 6 days after infection. At steady-state, there were few major *Ramp3*-dependent differences in gene expression, other than the predicted reduced expression in *Ramp3* transcripts in *Ramp3*$^{-/-}$ mice (**Extended Data** Fig. 3c, **Suppl. Table 1**). Infection caused a strong decrease of *Ramp3* transcripts in *Ramp3*$^{+/+}$ MAIT cells (**Extended Data** Fig. 3d). This suggested the hypothesis that decreased RAMP3 might be required for the increase in MAIT cells at this time after infection. After infection, there were additional major differences in gene expression in *Ramp3*$^{-/-}$ mice, with increased expression of genes related to autophagy and apoptosis, including *Stk17b*, *Gabarap*, *Foxo1* and *Fos*, but also genes related to cytokine-induced cell death, such as *Ifngr1*, *Jak1*, *F2r* and *Tgif1* (**Extended Data** Fig. 3c, **Suppl. Table 2**). Additionally, we detected several genes related to TCR signaling and immune activation to be increased in lung MAIT cells from *Ramp3*$^{-/-}$ mice, including *Ptprc*, *Cd8b1*, *Grap2*, *Lime1*, *Ccl5*, *Jaml*, *Selplg* and *Sla*. Using Ingenuity Pathway Analysis (IPA), there were several canonical pathways related to cell stress and apoptosis, as well as activation, enhanced in lung *Ramp3*$^{-/-}$ MAIT cells (Fig. 3c, **Suppl. Table 3**). We also analyzed predicted upstream regulators of these pathways with IPA, and found several genes or pathways related to TCR signaling were predicted to be upregulated in *Ramp3*$^{-/-}$ MAIT cells (**Extended Data** Fig. 3e, **Suppl. Table 4**). For example, *Ramp3*$^{-/-}$ MAIT cells had higher predicted signaling from *CD28*, *ITK*, and *PDK1*, all components of the TCR downstream signaling pathways [42]. Additionally, the predicted CD38 upstream modulation could indicate endothelial adhesion or metabolic regulation preferentially occurring in *Ramp3*$^{-/-}$ MAIT cells during activation [43]. Consistent with TCR activation, there was an increase in *Il17a* and *Ifng* transcripts in *Ramp3*$^{-/-}$ MAIT cells, although *Ccl5* was decreased (**Extended Data** Fig. 3f).

As RAMP proteins have been associated with adrenomedullin and calcitonin-related gene peptide (CGRP) signaling [44,45], we tested if transcripts for receptors for these proteins were expressed in MAIT cells after infection. There was very low expression of the *Calclr* gene in wild-type MAIT cells after infection, which was increased on *Ramp3*$^{-/-}$ MAIT cells (**Extended Data** Fig. 3g). Virtually no expression of transcripts encoding the alternative RAMP3-paired adrenomedullin receptor, *Ackr3*, were detected. This suggested that calcitonin gene related peptide and adrenomedullin signaling likely were not important for regulating lung MAIT cells.

Together, these data suggested that while MAIT cells rapidly increased in the lungs of both *Ramp3*$^{-/-}$ and control mice after pulmonary infection, in *Ramp3*$^{-/-}$ mice, these cells were more activated, produced more cytokines, but also were under stress, and less capable of long-term survival.

Increased bacterial load and tissue damage in the lungs of Ramp3$^{-/-}$ mice

Ramp3 $^{-/-}$ mice had increased lung MAIT cells at day 6, the peak of the effector response, with increased capability to produce IL-17A. Despite this, and the reported role of MAIT cells in clearing this infection [36,38], *Ramp3*$^{-/-}$ mice had a higher bacterial burden at day 6 after infection compared to both control mouse strains (Fig. 4a). We performed histological analysis of mouse lungs from *Ramp3*$^{-/-}$ and controls 6 days after *Salmonella* infection. By analyzing Hematoxylin and Eosin-stained full lung sections, we observed that infected *Ramp3*$^{-/-}$ mice had greater lymphocytic infiltrates surrounding airways and blood vessels in the lung compared to wild-type mice, a characteristic of histological bronchopneumonia (**Extended Data** Fig. 4a). Using these images, we trained a machine learning pixel classifier model to categorize tissue as “inflamed” or “non-inflamed”, based on infected or steady-state control slides that were evaluated by a veterinary pathologist. The criteria included regions with tissue damage, bronchopneumonia, cell infiltration, pleuritis, and alveolar hemorrhage (Fig. 4b, **Extended Data** Fig. 4b). We detected increased areas of inflammation in the infected lungs of both *Ramp3*$^{-/-}$ and *Ramp3*$^{+/-}$ mice (Fig. 4b). By flow cytometry, the number of neutrophils was also increased in the lungs of infected *Ramp3*$^{-/-}$ mice (Fig. 4c).

We performed immunofluorescent microscopy to characterize further the infiltration of cells into the lung tissue at day 6 after infection and the distribution of immune cells in proximity to bronchial airways and blood vessels (Fig. 4d, **Extended Data** Fig. 4c). There was an increased percentage of infiltrating T cells (CD3e^{+} cells), which are 25–35% MAIT cells, after infection in *Ramp3*$^{-/-}$ mice. Neutrophils (Ly6G^{+} cells) also were increased compared to both control strains, but macrophages, Iba1^{+} cells, were not elevated (Fig. 4e). In addition to total T lymphocytes, the average distance of T cells to bronchial airways in *Ramp3*$^{-/-}$ mice was decreased and the number of T cells in 50 μm from the perimeter of airways was increased compared to both control strains (Fig. 4f, **Extended Data** Fig. 4d**).** There were no differences comparing the accumulations or average distances close to blood vessels (Fig. 4f, **Extended Data** Fig. 4d).

To test whether this cellular infiltrate occurred exclusively in the parenchyma, we processed bronchial lavages (BAL) before harvesting the lungs. MAIT cells were increased in both the parenchymal and BAL fractions of the lungs of infected mice, with a larger number in the parenchyma (**Extended Data** Fig. 4e-f). The number of MAIT cells was increased in the parenchyma of both *Ramp3*$^{-/-}$ and *Ramp3*$^{+/-}$ infected mice compared to wild-type, but a difference based on *Ramp3* genotype was less evident in the BAL. We tested if MAIT cells from the parenchyma were accessible to an anti-CD45 antibody injected i.v. a short time before tissue harvest, to detect cells that are likely in the vasculature [46]. We did not observe many MAIT cells stained with i.v. CD45 in either parenchyma or BAL fractions, nor a difference in *Ramp3*$^{-/-}$ compared to control MAIT cells, indicating lung cells MAIT cells were not accessible to the vascular antibody. Compared to BAL, a higher percentage of lung MAIT cells in the parenchyma expressed CD103 (**Extended Data** Fig. 4f), which might be expected considering this integrin binds to E-cadherin [47], There was a significant reduction in the percentage of CD103^{+} MAIT cells in *Ramp3*$^{-/-}$ mice in the lung

parenchyma and BAL (**Extended Data** Fig. 4f), consistent with the analysis of the total population (**Extended Data** Fig. 2c).

We also tested lung infection with the *Streptococcus pneumoniae* strain URF918 (Fig. 4g). Clearance of *S. pneumoniae* is dependent on NKT17 cell antigen responses and gδ17 responses [48,49]. The highly virulent URF918 strain leads to rapid weight loss and the death of mice lacking iNKT cells within in one week [49]. *S. pneumoniae* produces a MAIT cell antigen [50]; however, lung MAIT cells are also activated within hours of infection, although the lung MAIT cell population does not increase greatly as in *Salmonella* BRD509 [38,49]. *Ramp3*$^{-/-}$ mice had a defective response, with more severe weight loss compared to control mice (Fig. 4h), as well as higher bacterial *S. pneumoniae* content at 2 days of infection compared to either control strain (Fig. 4i). There were also increased numbers of MAIT cells in the infected *Ramp3*$^{-/-}$ mice, although decreased iNKT cells after 15 h of infection (Fig. 4j). This may reflect a competition of these two cell types for a similar niche [51]. The increase in cell number corresponded with the number of cells producing IL-17 analyzed *ex vivo* (Fig. 4k), with increased IL-17-producing MAIT cells in *Ramp3*$^{-/-}$ mice, but decreased iNKT cells. Therefore, the response of *Ramp3*$^{-/-}$ mice to lung infection with *S. pneumoniae* exhibited features similar to the response to Salmonella BRD509, including a deleterious outcome with increased bacterial load and weight loss, coupled with increased MAIT cell number and activation of IL-17-producing lung MAIT cells.

These results indicate that the increased accumulation of activated MAIT cells detected in *Ramp3*$^{-/-}$ mice early after infection was accompanied not only by decreased bacterial clearance but also increased levels of neutrophil infiltration and tissue damage in the lungs.

RAMP3 influences surface CXCR6 expression by MAIT cells

CXCR6 is important for localization of CD4 and CD8 T cells to the lung [52–54]. Despite the direct correlation of *Ramp3* and *Cxcr6* transcripts in wild-type mice (Fig. 1b), analysis of low-input RNA-seq showed increased *Cxcr6* transcripts by lung MAIT cells in *Ramp3*$^{-/-}$ mice compared to both control strains at steady-state (**Extended Data** Fig. 5a). As RAMPs are involved in the trafficking of some GPCRs [25], we tested whether the absence of RAMP3 induced a difference in CXCR6 surface expression in T cells. At steady state, we detected higher cell surface expression of CXCR6 by lung MAIT cells from *Ramp3*$^{-/-}$ mice, but without increased surface expression or haploinsufficiency evident in *Cxcr6*$^{+/-}$ mice. There was also an increase in CXCR6 expression by MAIT thymocytes, and CXCR6 expression by lung and spleen iNKT cells was also increased in *Ramp3*$^{-/-}$ mice (Fig. 5a-b).

We tested if *Cxcr6* transcripts and CXCR6 surface protein expression were altered in infected *Ramp3*$^{-/-}$ mice and controls. From the RNA-seq data, *Cxcr6* transcripts were increased at day 6 after infection, but not selectively in *Ramp3*$^{-/-}$ mice (**Extended Data** Fig. 5b). Surface expression of CXCR6 was increased in both *Ramp3*$^{-/-}$ and control lung MAIT cells after infection, although it was highest in *Ramp3*$^{-/-}$ mice

(Fig. 5c). Similar to the steady-state situation, we did not detect significant changes in the surface levels of CXCR6 on other T cell populations after infection (Fig. 5d). By analyzing bronchial lavage and lung parenchyma, we tested whether increased CXCR6 expression by lung MAIT cells was dependent on lung location. The increase in cell surface expression of CXCR6 was most significant by lung MAIT cells from the parenchyma of *Ramp3*$^{-/-}$ mice, with less effect on MAIT cells in the bronchial lavage (**Extended Data** Fig. 5c).

CXCR6 recycles from the cell surface after exposure to its ligand, chemokine (C-X-C motif) ligand 16 (CXCL16) [55]. To test whether the higher surface levels of CXCR6 in lung MAIT cells from *Ramp3*$^{-/-}$ mice were due to increased synthesis or altered trafficking to the cell surface, we stained lung T cells from infected mice with anti-CXCR6 antibodies after permeabilization (Fig. 5e). The total CXCR6 protein detected after permeabilization was similar in *Ramp3*$^{-/-}$ and control mice, despite increased transcripts in the *Ramp3*$^{-/-}$ mice. This relative increase in CXCR6 on the cell surface of lung MAIT cells from *Ramp3*$^{-/-}$ mice, in the absence of an increase in total protein, is consistent with altered trafficking of this chemokine receptor, possibly the result of decreased CXCR6 internalization or increased recycling to the surface (Fig. 5e).

We next examined if over-expression of RAMP3 could regulate the surface expression of CXCR6 on the surface of lung MAIT cells. MAIT cells and conventional T cells (MR1:5OPRU^{neg}TCRβ^{+} cells) from *Salmonella*-exposed *Ramp3*$^{-/-}$ mice were transduced with a *Ramp3*-overexpression retrovirus (*Ramp3*-OE) or vector with empty cassette (eGFP-EV) and expanded *in vitro* for 5 days (Fig. 5f, **Extended Data** Fig. 5d). After expansion, the levels of CXCR6 in conventional T cells were not significantly altered, while CXCR6 expression was reduced in *Ramp3*-OE MAIT cells (Fig. 5g).

Increased MAIT cells in Ramp3 mice is CXCR6-dependent

To test if the increase in lung MAIT cells in *Ramp3*$^{-/-}$ mice after infection was dependent on a GPCR, we treated infected mice with Pertussis toxin, which inhibits all GPCRs using an α_i G protein for signaling. The MAIT cell accumulation in the lung of both wild-type and *Ramp3*$^{-/-}$ mice was greatly decreased by this toxin (Fig. 6a). We note that the average lung MAIT cell population after Pertussis toxin treatment, > 2×10^4 cells, was still increased compared to steady state (Fig. 1d). This could be due to incomplete blockade or the contribution of other mechanisms for the MAIT cell increase.

Chemokine receptors have diverse functions. Considering iNKT cells, CXCR6 has been implicated both in homing to the liver and in survival there [30,31]. To test if there is an effect of RAMP3 on CXCR6-CXCL16 mediated migration, we performed a transwell migration assay on the increased population of lung MAIT cells obtained after infection of wild-type and *Ramp3*$^{-/-}$ mice. When 50 μg/ml of CXCL16 were added to the lower chamber, no significant difference in migration was found between *Ramp3*$^{+/+}$ and *Ramp3*$^{-/-}$ MAIT cells (Fig. 6b). These data are consistent with results presented earlier indicating that migration of

MAIT cells to the lung over 4 days and/or their short-term survival was not increased by RAMP3 deficiency, despite the absence of RAMP3 in MAIT cells ultimately may allow accumulation of more cells in the lung at steady state or within days following acute infection (Fig. 1d, 2c).

To test the importance of CXCR6 for the increase in lung MAIT cells after infection, we analyzed *Cxcr6*$^{-/-}$ and control mice exposed to the *Salmonella* vaccine strain. There was a greatly reduced MAIT cell population expansion in the lungs of *Cxcr6*$^{-/-}$ mice, comparable to mice treated with Pertussis toxin, while MAIT cells in *Cxcr6*$^{+/-}$ mice were unaffected (Fig. 6c). The numbers of other immune cell populations were not affected by CXCR6 deficiency (Fig. 6d). To ascertain if this was due to the absence of CXCR6 expression by MAIT cells, we performed adoptive transfer experiments using *Cxcr6*$^{-/-}$ or *Cxcr6*$^{+/-}$ controls. MAIT cells were increased by prior infection, and the purified lung MAIT cells were transferred to *Rag1*$^{-/-}$ mice that were rechallenged with the same *Salmonella* strain and analyzed at day 6. There was a decreased accumulation of the previously activated *Cxcr6*$^{-/-}$ donor MAIT cells, both in the parenchyma and bronchial lavage of the recipients (Fig. 6e). To test a role for CXCR6 in the enhanced MAIT cell population in *Ramp3*$^{-/-}$ mice, infected mice were injected with an antibody to CXCL16, the only known ligand for CXCR6. Administration of this antibody partially blocked the increase in MAIT cells in *Ramp3*$^{-/-}$ mice (Fig. 6f), to a level below what was observed in infected wild-type mice. Taken together, these data indicate that RAMP3 can affect CXCR6 expression and some of the increased lung MAIT cells in *Ramp3*$^{-/-}$ mice is dependent not only GPCRs but specifically on CXCR6.

Discussion

Innate-like T cells are predominantly tissue-resident lymphocytes that are found at high concentrations in the lung and other tissues. In the mouse thymus, pre-formed functional subsets of innate-like T cells differentiate [56–58]. These thymus subsets, similar to CD4 Th1, Th2, and Th17 cells, are also found in the periphery, but there are tissue-specific differences in their frequencies [59]. For example, Th17-like cells are more prevalent in the lung and skin [33,60,61]. Despite this knowledge, little is known about the factors that positively or negatively regulate the location of these cells across different tissues. Here, we showed that the number of MAIT cells in the lung, predominantly MAIT17 cells, was limited or negatively regulated by RAMP3 and that, in its absence, MAIT cells were increased. Furthermore, their function was altered and *Ramp3*$^{-/-}$ mice had less effective early responses to acute lung bacterial infections. Our findings also showed that the chemokine receptor CXCR6 was a major factor required for the increased lung MAIT cell population after infection. Here we provided evidence that RAMP3 acted in part to regulate lung MAIT cells by regulating CXCR6.

RAMPs have diverse effects on the vasculature and metabolism, but only recently have they been reported to act in immune cells. Several publications show RAMPs involvement in immune cells is mediated by neuropeptides that engage heterodimers containing the CALCRL receptor, which changes specificity when paired with different RAMPs. This has been observed for several studies of (ILC2) [44,62–

[64]. In T cells, CGRP release by peripheral nerve cells decreases $CD8^+$ T cell activation, [29], and inhibits $CD8^+$ Th17 responses after exposure to commensal bacteria [65]. CGRP signaling promotes type 1 helper (Th1) differentiation in $CD4^+$ T cells [45]. This study implicates a receptor composed of CALCRL and RAMP3, despite a much lower affinity for CGRP than the CALCRL-RAMP1 receptor.

In contrast to these prior reports, the evidence here indicated that RAMP3 influences lung MAIT cells and the lung immune response by a different mechanism, in part by modulating CXCR6. We initially hypothesized that the transcriptional co-regulation of *Cxcr6* and *Ramp3* in wild-type mouse lung MAIT cells might be functional, given the ability of RAMP3 to bind CXCR6 [22] and the importance of CXCR6 for tissue-resident CD4 and CD8 T cells [52,66,67]. Furthermore, the PSD-95/Discs-large/ZO-1 homology (PDZ) domain, unique in RAMPs to RAMP3 is involved in GPCR trafficking and internalization [22,68], Indeed, the surface level of CXCR6 was increased in lung and thymus MAIT cells from *Ramp3*$^{-/-}$ mice. Furthermore, RAMP3 overexpression decreased CXCR6 expression by MAIT cells.

Our data showed lung MAIT cells were increased in *Ramp3*$^{-/-}$ mice both at steady-state and rapidly after acute infection. The reason for this selective effect is unknown, but it correlated with the increased transcription of *Ramp3* in lung MAIT cells. At steady-state, in vitro assays and cell transfers did not support an effect of RAMP3 directly on CXCR6-mediated homing. This is consistent with the finding that CXCR6 has a substitution of phenylalanine for the aspartic acid-arginine-tyrosine or DRY motif found in most chemokine receptors, a motif which plays a role in cell adhesion but reduces chemotaxis [55]. After infection, the large increase in lung MAIT cells in wild-type mice was due predominantly to *in situ* proliferation, in agreement with earlier reports [18,40]. The same was less evident in *Ramp3*$^{-/-}$ mice. The data were not consistent, however, with an effect of FTY720 on MAIT cells draining from the mediastinal lymph node to the lung. An effect of FTY720 on migration from the thymus or other lymph nodes cannot be excluded; FTY720 has been shown to prevent migration of MAIT cell subpopulations from the thymus in uninfected mice [35]. By day 6, the increased MAIT cell population in *Ramp3*$^{-/-}$ mice was activated but showed decreased proliferation and was in decline. These data suggest that despite increased MAIT cells at effector time point, the increased population was under stress and not sustainable.

In addition to changes in MAIT cell dynamics, there were also changes in lung MAIT cell functionality in *Ramp3*$^{-/-}$ mice. After infections, lung MAIT cells were more capable of secreting IL-17A. Despite this, the protective response was impaired and following *S. typhimurium* infection, the lungs showed signs of immunopathology. The dysfunctional lung immune response by *Ramp3*$^{-/-}$ MAIT cells could be secondary to the increased bacterial load and inflammation. Immunopathology may have resulted from the increased MAIT17 response to *Salmonella*, inappropriate for this intracellular bacterium. Host protection against *S. pneumoniae* lung infection requires IL-17A from innate-like T cells [49,69], however, *Ramp3*$^{-/-}$ mice had a higher bacterial burden. The number of NKT17 cells was reduced, and it is possible that these cells play a non-redundant role [49].

We demonstrated that CXCR6 is important for much of the large numerical increase in lung MAIT cells after *Salmonella* infection, the number gδ T cells or iNKT cells was not affected. In contrast, a previous report showed that the increase in MAIT cells after *F. tularensis* infection was not greatly affected in *Cxcr6*$^{-/-}$ mice, except for a decrease in bronchiolar lavage fluid evident by day 54 [18]. This may reflect differential requirements for CXCR6 by MAIT1 cells, preferentially expanded by *F. tularensis* [37], or the route of infection, intranasal as opposed to retropharyngeal aspiration. The previous report analyzes transgenic mice expressing the invariant MAIT cell TCR α chain [18], and these MAIT cells could have different properties.

A striking haploinsufficiency was evident in *Ramp3*$^{+/-}$ mice, evidenced by increased lung MAIT cell numbers, indicating a limitation in available RAMP3, which binds with many GPCRs. Analysis of *Ramp2*$^{+/-}$ mice likewise shows haploinsufficiency, with postnatal lethality and changes in the female reproductive tract, although these defects were less severe than the midgestational lethality in homozygous *Ramp2*$^{-/-}$ mice [70].

Blockade of the CXCR6 ligand CXCL16 reduced the boost in lung MAIT cell numbers in infected *Ramp3*$^{-/-}$ mice. These data connect the effects observed on lung MAIT cells in *Ramp3*$^{-/-}$ mice after infection to CXCR6. The simple interpretation of RAMP3 inhibiting the surface expression of CXCR6 as the sole means to regulate lung MAIT cells is confounded by the analysis of *Ramp3*$^{+/-}$ mice, which did not show increased surface expression. The *Ramp3*$^{+/-}$ mouse phenotype is intermediate, similar to *Ramp3*$^{-/-}$ mice for the increase in MAIT cells and other measures, but similar to wild-type mice for reduction in some inflammatory parameters, such as CFU in the lung, number of neutrophils and infiltrating T cells, and reduced apoptosis in MAIT cells. It is possible that in *Ramp3*$^{+/-}$ mice the recycling or re-sensitization of CXCR6 were enhanced, despite a lack of increased surface expression. The involvement of other GPCRs, or other mechanisms due to RAMP3 expression, cannot be excluded.

Here, we have identified two proteins expressed by mouse lung MAIT cells that specifically regulated the size and function of the predominantly MAIT17 population, both at steady state and during the substantial increase after infection. We showed that CXCR6 is important for the largely in situ increase in lung MAIT cells that occurred after certain bacterial infections. The MAIT cell population was counter-regulated by RAMP3, acting through CXCR6, but likely additional mechanisms. We showed that RAMP3 influenced the function of MAIT cells after infection, with important implications for host defense. Together with earlier publications on immune responses, and their known ability to interact with many GPCRs, the data suggest that additional effects of RAMP proteins on immune responses are likely to be discovered.

Materials and methods

Analysis of public single cell transcriptomic dataset

A single cell dataset deposited in NCBI GEOBUS with accession number GSE189484 was used to analyze expression of *Ramp* transcripts by mouse MAIT cells. Analysis was performed on Seurat v5 using the same parameters as described in Chandra et al. 2023 [4].

Mice

Ramp3$^{-/-}$ mice were previously generated [23] and bred with the 129S6/SvEv background strain (Taconic Biosciences). C57BL/6, Ly5.1 congenic (B6.SJL-*Ptprc*^{a}*Pepc*^{b}/BoyJ), *Rag1*$^{-/-}$ (B6;129S7-*Rag1*^{tmMom}/J) and *Cxcr6*$^{-/-}$ (B6.129P2-*Cxcr6*^{tm1Litt}/J) mice were purchased from Jackson labs. Mice were bred in the vivarium at the La Jolla Institute for Immunology. Male and female mice were used at 8–14 weeks of age. All procedures were approved by the La Jolla Institute for Immunology Institutional Animal Care and Use Committee and were compliant with the ARRIVE standards.

Tissue processing

Lungs were digested with spleen dissociation media (STEMCELL) and mechanical disruption using the GentleMACS Dissociator (Miltenyi). Ears were removed from the base of the cartilage, and dermis and epidermis were mechanically separated with fine forceps. Ear skin was digested in 0.25 ug/ml of Liberase TL (Roche) for 1 h and 45 min at 37˚C. Skin cells were then treated in 2.7 ug/ml DNase (Sigma-Aldrich) and 0.01 M EDTA. Skin cells, splenocytes, thymocytes and liver cells were harvested by mechanical disruption on a 70 μm cell strainer. Liver cells were additionally separated in a 34% Percoll gradient. To obtain cells from bronchial-alveolar lavage, lungs were flushed 2 times with 1 ml of cold PBS through the trachea before harvesting the lung. All cells were treated with RBC lysis buffer (Sigma-Alrich) and washed with HBSS 10% FBS.

Bone marrow chimeras

Ly5.1 mice were X-ray irradiated with 900 rads and reconstituted i.v. with 10 x 10^6 bone marrow cells from either *Ramp3*$^{+/+}$ or *Ramp3*$^{-/-}$ mice depleted with anti-CD4 and anti-CD8 antibodies. Lung, liver and spleen were harvested after 120 days and analyzed by flow cytometry.

Salmonella enterica BRD509 infection

All infections were carried out with an attenuated strain of *Salmonella enterica serovar Typhimurium* BRD509, a gift from Dr. Stephen P. Schoenberger (La Jolla Institute for Immunology, La Jolla, CA)[71]. Overnight cultures were grown in Luria broth (LB) with 100 μg/ml of Streptomycin, then sub-cultured the next day for 4 h to mid-log phase. An inoculum of 1 x 10^6 CFU per mouse in PBS were administered by retropharyngeal injection. Dose was confirmed by plating serial dilutions on LB agar plates. Mice were analyzed at 6 days after infection, unless otherwise noted.

Flow cytometry and cell sorting

MR1 tetramers loaded with 5-OP-RU were obtained from the NIH Tetramer Core Facility. Single cell suspensions were stained with tetramers for 30 min at 4˚C. Cells were stained with Live/Dead Yellow

(ThermoFisher) or Live/Dead Ghost UV450 (Cytek Biosciences) at 1:1000 or 1:500 dilutions, respectively, and blocked with anti-CD16/32 (2.4G2) antibody at 1:500 and free streptavidin at a 1:1000 dilution in PBS for 15 min at 4˚C. After washing, cells were stained with cell surface-specific antibodies for 30 min at 4˚C. For intracellular cytokine staining, cells were previously stimulated with 100 ng/ml of PMA and 1 µg/ml of Ionomycin for 2h at 37˚C and then incubated in GolgiStop and GolgiPlug (BD Pharmingen) for 2 h at 37˚C. Re-stimulation with PMA and Ionomycin was not performed in the experiments indicated as Brefeldin A only. For intracellular staining, cells were fixed with CytoFix (BD) for 20 min and permeabilized with Perm 1X solution (ThermoFisher) with intracellular antibodies overnight at 4˚C. For flow cytometry experiments, data were acquired on Cytek Aurora (Cytek Biosciences) or FACS Symphony S6 (BD Biosciences). Data were analyzed with FlowJo v10.7 (BD Bioscience). For sorting experiments, cells were sorted on either FACS Symphony S6 or FACS Aria (BD Biosciences). A complete list of antibodies and flow cytometry reagents are available on **Supplementary Table 5**.

Adoptive transfer

Wild-type, *Ramp3*$^{-/-}$ or *Cxcr6*$^{-/-}$ mice were infected with BRD509 as described above to expand the MAIT cell population in the lung. MAIT cells were then sorted and washed in sterile PBS and 2 x 10^5 cells were injected into each recipient mouse.

In vivo migration assay

Sorted *Ramp3*$^{+/+}$ MAIT cells were stained CFSE (ThermoFisher) while *Ramp3*$^{-/-}$ or *Ramp3*$^{+/-}$ MAIT cells were stained with CellTrace Violet (ThermoFisher) according to manufacturer instructions. Labeled cells and co-transferred into *Ramp3*$^{+/+}$ mice. Spleen and lung were analyzed 4 days after transfer.

Vascular accessibility staining

Mice were anaesthetized with isoflurane and injected with 3 µg of BV785-labeled anti-CD45 antibody (clone 30-F11), as described previously. Tissues were harvested within 3 minutes.

BrdU incorporation

Together with infection, mice were intraperitoneally injected with 100 µl of 10 mg/ml 5-bromo-2'-deoxyuridine (BrdU) in sterile DPBS. After 6 days, lung cells were collected and processed as described above. After staining and fixing steps, cells were permeabilized with BD CytoPerm Permeabilization Buffer Plus for 10 min at 4˚C. Cells were then washed and fixed again with BD CytoFix Buffer for an additional 5 min at 4˚C. Cells were then treated with 300ug/ml of DNase I for 1h at 37˚C. Cells were then stained with anti-BrdU antibodies for 20 min at room temperature, washed and analyzed by flow cytometry.

Apoptosis measurement

After infection, lung cells were processed and resuspended in PBS. Cells were then treated with CellEvent® Caspase-3/7 Green Detection Reagent for 45 min at room temperature in the dark. After

incubation, cells were stained with SYTOX® AADvanced™ dead cell solution for an additional 5 min at 37˚C.

Histology and Microscopy

Whole lungs of control and infected mice were flushed and fixed with zinc formalin (Medical Chemical Corp.) at room temperature for 24 hours and embedded in paraffin for sectioning 4 µm slides. Hematoxylin and Eosin-stained slides were scanned on a Zeiss Axio Scan with a 40x/0.95 objective. Slides were qualitatively surveyed for areas of inflammation by a board-certified veterinary histopathologist (K.K.). The pathologist noted lesions of bronchopneumonia, neutrophil infiltration, pleuritis, and alveolar hemorrhage. The pathologist trained the study team on identification of these lesions and anatomic landmarks. The study team annotated areas training a Random-tree based Pixel classifier on QuPath v0.5.0. Immunofluorescent staining was performed followed by antigen retrieval with sodium citrate buffer (10 mM sodium citrate and 0.05% Tween 20, pH 6.0). Tissue sections were treated with 10% normal donkey serum (Jackson ImmunoResearch) and stained with antibodies in antibody dilution buffer supplemented with 0.3% Triton X-100 (Sigma-Aldrich) and 1% BSA. Secondary antibodies were purchased from Invitrogen. Samples were mounted with Prolong Gold (ThermoFisher Scientific), and images of representative tissues were captured by Zeiss Axio Scan slide scanner microscope and analyzed with Zen software (Carl Zeiss). Cell segmentation of immunofluorescent images and cell classification was performed in QuPath v0.5.0 using StarDist extension v0.5.0.

Treatments of Infected mice

For $G\alpha_i$ inhibition, 200 ng of Pertussis toxin (List Labs) or 100 µl of PBS were injected intravenously every 2 days into each mouse starting at the same time as infection. For CXCR6 blockade, 100 µg of anti-mouse CXCL16 antibody (clone 142417, ThermoFisher) or IgG isotype control were injected intravenously per mouse every 2 days into each mouse starting at the same time as infection. For lymphatic migration inhibition, 25 µg of sphingosine-1-phosphate receptor agonist FTY720 (Sigma-Aldrich) or 100 µl of PBS were injected intraperitoneally into each mouse every day starting at the same time as infection. For all experiments, mice were analyzed at day 6 by flow cytometry.

MSCV cloning and transduction

MSCV-GFP-EV and MSCV-IRES-CD90.1 retroviral backbones were kindly provided by Wade Zhang (La Jolla Institute for Immunology). Mouse *Ramp3* cDNA was cloned from pCMV-SPORT6 plasmid purchased from TransOmics to generate the MSCV-*Ramp3*-OE plasmid. HEK293T cells were co-transfected with MSCV plasmids and pCL-Eco at a 1:3 molar ratio with Trans-IT reagent (Muris) in Opti-MEM media (ThermoFisher). Viral supernatant was either used fresh or stored at -80˚C before use. Spleen conventional T cells were isolated by MACS (STEMCELL) and activated with plate-bound anti-CD3/CD28 for 24 h with mouse recombinant IL-2 (Peprotech). Cells were then transduced with 70% viral supernatant with 10 µM of Probenecid (Sigma-Alrich) and centrifuged at 2000 *g* for 2 h at 37˚C. Cells were analyzed 5 days after transduction.

Western blot

Over-expression of RAMP3 was confirmed by western blot using transduced spleen $CD4^+$ and $CD8^+$ T cells isolated by magnetic cell separations (MACS). For each sample, 40 µg of total protein was loaded on to 7.5% SDS-PAGE gel and then transferred to a nitrocellulose membrane. Membranes were blocked with 5% BSA in Tris-buffered saline with Treen-20 (TBST) on a rocking table for 1h at room temperature and stained overnight with 1:500 dilution of rabbit polyclonal anti-RAMP3 antibody (ABclonal) in 2.5% BSA TBST overnight at 4˚C. Secondary antibodies were incubated at 1h at room temperature and chemiluminescent reagents were added to the membrane for 1 min at room temperature. Pseudo-quantification and analysis were done using Fiji ImageJ software normalizing against β-actin as a loading control.

CXCL16 transwell migration assay

BRD509-expanded lung MAIT cells were sorted and activated with plate-bound anti-CD3/CD28 and cultured for 24 h with mouse recombinant IL-2 (Peprotech). Cells were then seeded in top transwell and then placed into the bottom transwell with or without 50 µg/ml of mouse recombinant CXCL16 (Peprotech) for 24h at 37˚C 5% CO_2. After incubation, the top transwell was carefully retrieved and cells migrating to lower chamber were counted on Vi-CELL automated Cell Counter (Beckman Coulter).

Bulk RNA sequencing

At least 10^4 MAIT cells were isolated by cell sorting using a FACS Aria instrument by pooling cells from 5 to 10 mice. RNA extraction was performed using RNAeasy mini kit (Qiagen). RNA-seq libraries were prepared using SMARTer stranded total RNA-seq kit v2 (Takara). Libraries were sequenced using an Illumina NovaSeq 6000 to generate 50-bp paired-end reads. Three biological replicates were generated for each condition. Reads were mapped to the mm10 reference genome using Kallisto v0.52. After quality control, all samples had more than 80% of their reads mapped. Differential gene expression was calculated using DESeq2 (v1.38.3) in an R environment (v4.2.2). Significant differential expression was defined as $\log_2$ fold-change higher than 1.0 and a Benjamini-Hochberg-adjusted *p*-value lower than 0.05.

Pathway analysis and upstream regulator analysis

Canonical pathway analysis as well as upstream regulators associated to these pathways were calculated using the Ingenuity Pathway Analysis (IPA, Qiagen) knowledge-based database graphical user interface (GUI). The generated z-scores and adjusted p-values for each pathway and upstream regulator can be found in the Supplementary Tables.

Statistical analysis

All data were shown as mean ± standard error (s.e.m) as stated in the figure legends. Statistical significance was determined by unpaired two-tailed Student's t test, or one-way or two-way ANOVA with post-hoc Tukey's multiple comparison test. All flow cytometry and histology data were analyzed in GraphPad Prism v10 (GraphPad).

Declarations

Code and data availability

All code generated from bioinformatic analysis from this study has been deposited in this GitHub repository: https://github.com/gabrielascui/Ramp3KO_bRNAseq. Bulk RNA-seq dataset has been deposited in the NCBI GEO repository GSE341649. Full western blot images are contained in this repository: https://doi.org/10.5281/zenodo.21845137.

Acknowledgements

We would like to acknowledge C. Kim, D. Hinz, and C. Dillingham from the LJI Flow Cytometry Core Facilities for their assistance with cell sorting. We thank S. Alarcón and H. Dose of the LJI NGS Core Facilities on their assistance with library preparation and sequencing on the NovaSeq 6000. We thank Z. Mikulski of the LJI Microscopy Core Facilities for his assistance in tissue preparation and data acquisition.

Author contribution

The study was conceptualized by SC, GA and MK. Experiments were performed by GA, EP, AM, PG, CL, DH, JH, and XW. Histological data analysis was performed by AM, KK, SM and GA. Bioinformatic analysis was done by GA. SM, AM and KK performed histological analysis and generated machine learning algorithms. Cloning was performed by AB and viral production was done by CL. GA, MK, MC and KC wrote, edited and reviewed the manuscript.

Funding

This project was supported by R01 5R01AI137230-03 grant, P30 DK120515 SDDRC. Institutional instrument grants S10 RR027366 and S10 OD025052 were awarded to La Jolla Institute for Immunology. GA received an ARCS Scholar fellowship from ARCS Foundation, San Diego Chapter.

References

1. Salou M et al (2019) A common transcriptomic program acquired in the thymus defines tissue residency of MAIT and NKT subsets. J Exp Med 216:133–151

2. Dusseaux M et al (2011) Human MAIT cells are xenobiotic-resistant, tissue-targeted, CD161hi IL-17–secreting T cells. Blood 117:1250–1259
3. Wu Z, Chen X, Han F, Leeansyah E (2025) MAIT cell homing in intestinal homeostasis and inflammation. Sci Adv 11:eadu4172
4. Chandra S et al (2023) Transcriptomes and metabolism define mouse and human MAIT cell populations. Sci Immunol 8:eabn8531
5. Gherardin NA et al (2018) Human blood MAIT cell subsets defined using MR1 tetramers. Immunol Cell Biol 96:507–525
6. Legoux F et al (2019) Microbial metabolites control the thymic development of mucosal-associated invariant T cells. Science 2719:eaaw2719
7. Legoux F et al (2019) Molecular mechanisms of lineage decisions in metabolite-specific T cells. Nat Immunol 20:1244–1255
8. Chandra S et al (2018) Development of Asthma in Inner-City Children: Possible Roles of MAIT Cells and Variation in the Home Environment. J Immunol 200:1995–2003
9. Lezmi G et al (2019) Evidence for a MAIT-17–high phenotype in children with severe asthma. J Allergy Clin Immunol 144:1714–1716e6
10. Lu B et al (2020) IL-17 production by tissue-resident MAIT cells is locally induced in children with pneumonia. Mucosal Immunol 13:824–835
11. Constantinides MG et al (2019) MAIT cells are imprinted by the microbiota in early life and promote tissue repair. Science 366
12. Zheng Y et al (2024) MAIT cell activation and recruitment in inflammation and tissue damage in acute appendicitis. Sci Adv 10:eadn6331
13. El Morr Y et al (2024) MAIT cells monitor intestinal dysbiosis and contribute to host protection during colitis. Sci Immunol 9:eadi8954
14. Hartmann N et al (2018) Role of MAIT cells in pulmonary bacterial infection. Mol Immunol 101:155–159
15. Meermeier EW et al (2022) Human lung-resident mucosal-associated invariant T cells are abundant, express antimicrobial proteins, and are cytokine responsive. Commun Biol 5:1–13
16. Voillet V et al (2018) Human MAIT cells exit peripheral tissues and recirculate via lymph in steady state conditions. JCI Insight 3
17. Wang H et al (2019) IL-23 costimulates antigen-specific MAIT cell activation and enables vaccination against bacterial infection. Sci Immunol 4:eaaw0402
18. Yu H et al (2020) CXCL16 Stimulates Antigen-Induced MAIT Cell Accumulation but Trafficking During Lung Infection Is CXCR6-Independent. Front Immunol 11
19. Serafin DS, Harris NR, Nielsen NR, Mackie DI, Caron KM (2020) Dawn of a New RAMPage. Trends Pharmacol Sci 41:249–265

20. Armour SL, Foord S, Kenakin T, Chen W-J (1999) Pharmacological characterization of receptor-activity-modifying proteins (RAMPs) and the human calcitonin receptor. J Pharmacol Toxicol Methods 42:217–224
21. Mackie DI et al (2018) hCALCRL mutation causes autosomal recessive nonimmune hydrops fetalis with lymphatic dysplasia. J Exp Med 215:2339–2353
22. Mackie DI et al (2019) RAMP3 determines rapid recycling of atypical chemokine receptor-3 for guided angiogenesis. *Proc. Natl. Acad. Sci.* 116, 24093 LP – 24099
23. Dackor R, Fritz-Six K, Smithies O, Caron K (2007) Receptor Activity-modifying Proteins 2 and 3 Have Distinct Physiological Functions from Embryogenesis to Old Age*. J Biol Chem 282:18094–18099
24. Kim J et al (2020) Altered Expression of Adrenomedullin 2 and its Receptor in the Adipose Tissue of Obese Patients. J Clin Endocrinol Metab 105:e583–e596
25. Lorenzen E et al (2019) Multiplexed analysis of the secretin-like GPCR-RAMP interactome. Sci Adv 5:eaaw2778
26. Murray MP et al (2021) Transcriptome and chromatin landscape of iNKT cells are shaped by subset differentiation and antigen exposure. Nat Commun 12:1–14
27. Miragaia RJ et al (2019) Single-Cell Transcriptomics of Regulatory T Cells Reveals Trajectories of Tissue Adaptation. Immunity 50:493–504e7
28. Park SL et al (2023) Divergent molecular networks program functionally distinct CD8 + skin-resident memory T cells. Science 382:1073–1079
29. Darragh LB et al (2024) Sensory nerve release of CGRP increases tumor growth in HNSCC by suppressing TILs. Med 5:254–270e8
30. Geissmann F et al (2005) Intravascular immune surveillance by CXCR6 + NKT cells patrolling liver sinusoids. PLoS Biol 3:0650–0661
31. Germanov E et al (2008) Critical Role for the Chemokine Receptor CXCR6 in Homeostasis and Activation of CD1d-Restricted NKT Cells. J Immunol 181:81–91
32. Lamichhane R et al (2021) Human liver-derived MAIT cells differ from blood MAIT cells in their metabolism and response to TCR-independent activation. Eur J Immunol. https://doi.org/10.1002/eji.202048830
33. du Halgouet A et al (2023) Role of MR1-driven signals and amphiregulin on the recruitment and repair function of MAIT cells during skin wound healing. Immunity 56:78–92e6
34. Yoshida H et al (2019) The cis-Regulatory Atlas of the Mouse Immune System. Cell 176:897–912e20
35. Paiva RA et al (2026) MAIT cells egress the thymus at several maturation stages with selective capacity to seed different tissues. Immunity 0
36. Chen Z et al (2017) Mucosal-associated invariant T-cell activation and accumulation after in vivo infection depends on microbial riboflavin synthesis and co-stimulatory signals. Mucosal Immunol 10:58–68

37. Zhao Z et al (2021) Francisella tularensis induces Th1 like MAIT cells conferring protection against systemic and local infection. Nat Commun 12:4355
38. Riffelmacher T et al (2023) Divergent metabolic programmes control two populations of MAIT cells that protect the lung. Nat Cell Biol 25:877–891
39. Ataide MA et al (2022) Lymphatic migration of unconventional T cells promotes site-specific immunity in distinct lymph nodes. Immunity 1–16. 10.1016/j.immuni.2022.07.019
40. Wang H et al (2024) MAIT cell plasticity enables functional adaptation that drives antibacterial immune protection. Sci Immunol 9:eadp9841
41. Rahimpour A et al (2015) Identification of phenotypically and functionally heterogeneous mouse mucosal-associated invariant T cells using MR1 tetramers. J Exp Med 212:1095–1108
42. Shah K, Al-Haidari A, Sun J, Kazi J (2021) U. T cell receptor (TCR) signaling in health and disease. Signal Transduct Target Ther 6:412
43. Chatterjee S et al (2018) CD38-NAD+Axis Regulates Immunotherapeutic Anti-Tumor T Cell Response. Cell Metab 27:85–100e8
44. Han J et al (2022) Hypoxia induces adrenomedullin from lung epithelia, stimulating ILC2 inflammation and immunity. J Exp Med 219:e20211985
45. Hou Y et al (2024) Neuropeptide signalling orchestrates T cell differentiation. Nature 635:444–452
46. Anderson KG et al (2014) Intravascular staining for discrimination of vascular and tissue leukocytes. Nat Protoc 9:209–222
47. Cepek KL et al (1994) Adhesion between epithelial cells and T lymphocytes mediated by E-cadherin and the αEβ7 integrin. Nature 372:190–193
48. Hassane M et al (2020) Interleukin-7 protects against bacterial respiratory infection by promoting IL-17A-producing innate T-cell response. Mucosal Immunol 13:128–139
49. Murray MP et al (2022) Stimulation of a subset of natural killer T cells by CD103 + DC is required for GM-CSF and protection from pneumococcal infection. Cell Rep 38
50. Hartmann N et al (2018) Riboflavin Metabolism Variation among Clinical Isolates of Streptococcus pneumoniae Results in Differential Activation of Mucosal-associated Invariant T Cells. Am J Respir Cell Mol Biol 58:767–776
51. Koay HF et al (2016) A three-stage intrathymic development pathway for the mucosal-associated invariant T cell lineage. Nat Immunol 17:1300–1311
52. Heim TA et al (2025) CXCR6 promotes dermal CD8 + T cell survival and transition to long-term tissue residence. *J. Immunol.* vkaf219 10.1093/jimmun/vkaf219
53. Hou L, Yuki K (2022) CCR6 and CXCR6 Identify the Th17 Cells With Cytotoxicity in Experimental Autoimmune Encephalomyelitis. Front Immunol 13
54. Pilato MD et al (2021) CXCR6 positions cytotoxic T cells to receive critical survival signals in the tumor microenvironment. Cell 184:4512–4530e22

55. Koenen A et al (2017) The DRF motif of CXCR6 as chemokine receptor adaptation to adhesion. PLoS ONE 12:e0173486
56. Crosby CM, Kronenberg M (2018) Tissue-specific functions of invariant natural killer T cells. Nat Rev Immunol 18:559–574
57. Mayassi T, Barreiro LB, Rossjohn J, Jabri B (2021) A multilayered immune system through the lens of unconventional T cells. Nature 595:501–510
58. Pellicci DG, Koay HF, Berzins SP (2020) Thymic development of unconventional T cells: how NKT cells, MAIT cells and γδ T cells emerge. Nat Rev Immunol. https://doi.org/10.1038/s41577-020-0345-y
59. Harly C, Robert J, Legoux F, Lantz O (2022) γδ T, NKT, and MAIT Cells During Evolution: Redundancy or Specialized Functions? J Immunol 209:217–225
60. Hackstein C-P, Klenerman P (2023) MAITs and their mates: Innate-like behaviors in conventional and unconventional T cells. Clin Exp Immunol 213:1–9
61. López-Rodríguez JC, Barral P (2024) Mucosal associated invariant T cells: Powerhouses of the lung. Immunol Lett 269:106910
62. Nagashima H et al (2019) Neuropeptide CGRP Limits Group 2 Innate Lymphoid Cell Responses and Constrains Type 2 Inflammation. Immunity 51:682–695e6
63. Wallrapp A et al (2019) Calcitonin Gene-Related Peptide Negatively Regulates Alarmin-Driven Type 2 Innate Lymphoid Cell Responses. Immunity 51:709–723e6
64. Xu H et al (2019) Transcriptional Atlas of Intestinal Immune Cells Reveals that Neuropeptide α-CGRP Modulates Group 2 Innate Lymphoid Cell Responses. Immunity 51:696–708e9
65. Kulalert W et al (2024) The neuroimmune CGRP–RAMP1 axis tunes cutaneous adaptive immunity to the microbiota. *Proc. Natl. Acad. Sci.* 121, e2322574121
66. Ji J et al (2025) CXCR6 defines a distinct resident state in γδ T cells for protecting from liver cirrhosis. Hepatology 10 1097/HEP.
0000000000001643
67. Wein AN et al (2019) CXCR6 regulates localization of tissue-resident memory CD8 T cells to the airways. J Exp Med 216:2748–2762
68. Bomberger JM, Spielman WS, Hall CS, Weinman EJ, Parameswaran N (2005) Receptor Activity-modifying Protein (RAMP) Isoform-specific Regulation of Adrenomedullin Receptor Trafficking by NHERF-1 *. J Biol Chem 280:23926–23935
69. Xu R et al (2023) TNFR2 + regulatory T cells protect against bacteremic pneumococcal pneumonia by suppressing IL-17A-producing γδ T cells in the lung. Cell Rep 42:112054
70. Kadmiel M et al (2011) Research Resource: Haploinsufficiency of Receptor Activity-Modifying Protein-2 (Ramp2) Causes Reduced Fertility, Hyperprolactinemia, Skeletal Abnormalities, and Endocrine Dysfunction in Mice. Mol Endocrinol 25:1244–1253

71. Tacket CO et al (1997) Safety of live oral Salmonella typhi vaccine strains with deletions in htrA and aroC aroD and immune response in humans. Infect Immun 65:452–456

Figures

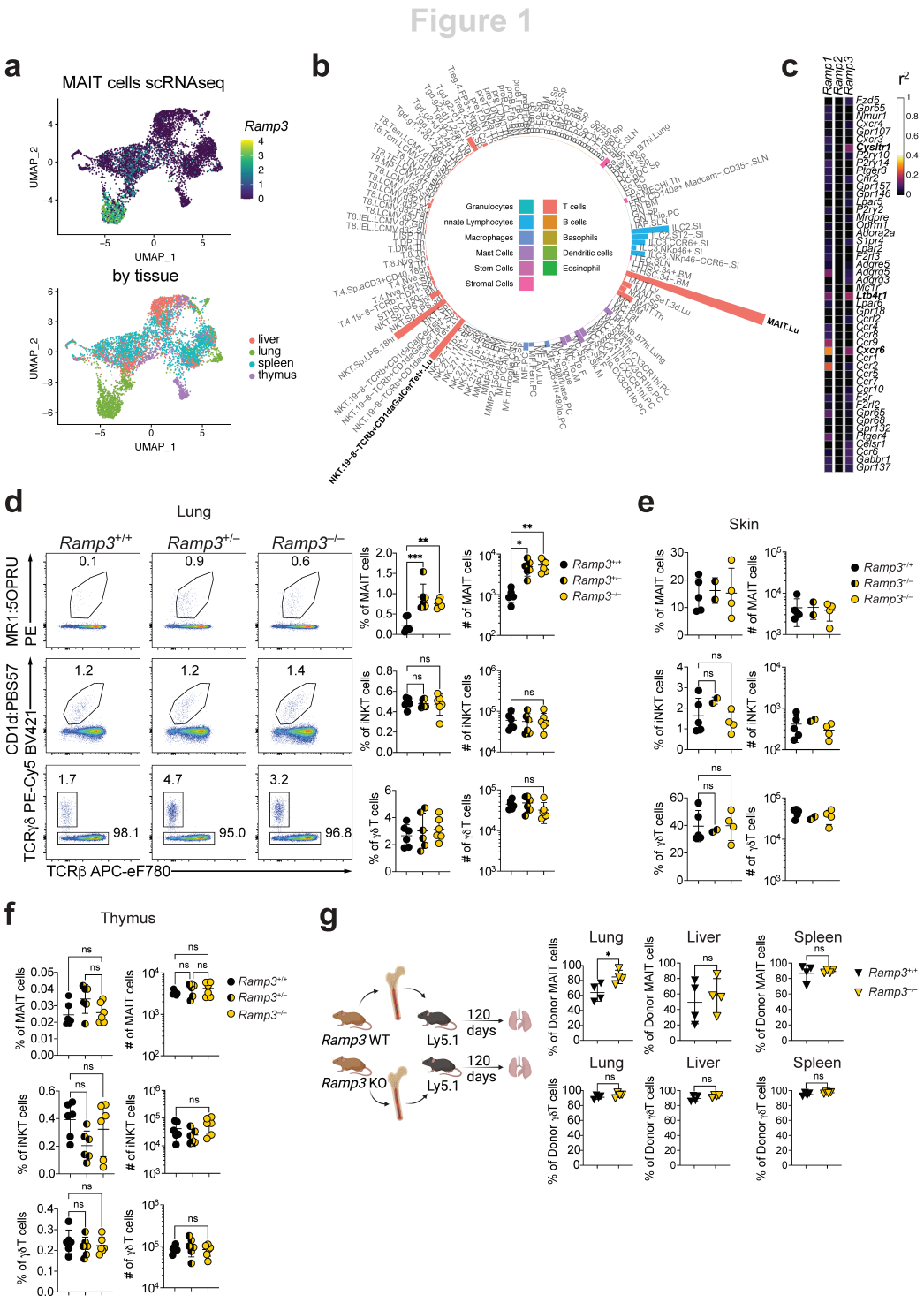


Figure 1

Lung MAIT cells have high expression of *Ramp3* and are increased in *Ramp3*$^{-/-}$ mice

a) Published single cell transcriptomic analysis of MAIT cells from several tissues [4]. *Ramp3* expression by MAIT cells (*top*) and tissue of origin of the MAIT cells in each cluster (*bottom*). **b)** *Ramp3* expression (TPM) by different lymphocyte populations from C57BL/6 mice. Data from the ImmGEN Consortium ultra-low input bulk-RNA sequencing. CD19^{-}, CD8^{-} NKT cells and MAIT cells are indicated in bold font. Lu: lung; Lv: liver; Sp: spleen; Th: Thymus. Other abbreviations are described on the ImmGEN portal (immgen.org). **c)** Lung MAIT cells were evaluated by Spearman correlations for expression of *Ramp3* and GPCR genes present in the scRNA-seq dataset. **d)** (*left*) flow cytometry of gd T cells, iNKT cells, and MAIT cells from the lungs of *Ramp3*$^{-/-}$, heterozygous and wild-type mice at steady-state. (*right*) accumulated data from steady-state lungs of *Ramp3*$^{-/-}$ mice. n = 6 for each group. **e)** Skin of *Ramp3*$^{-/-}$ and control mice. n = 5;2;4 per wild-type, heterozygous and knockout, respectively. **f)** Accumulated flow cytometry data of the indicated T cell populations from the thymus. n = 6 for each group. Lines indicate mean ± SE. Data analyzed by one-way ANOVA with post-hoc Tukey or Krustal-Wallis with post-hoc Dunn's Test for multiple comparisons. ***: $p < 0.001$, **: $p < 0.01$, *: $p < 0.05$, ns: $p \geq 0.05$. **g)** Bone marrow chimeras were generated with wild-type or *Ramp3*$^{-/-}$ donors and analyzed after 120 days for the percentage of donor-derived cells in total MAIT or gd T cells, respectively. n = 4 per group. Lines indicate mean ± SE. Data analyzed by two-tailed unpaired t test. *: $p < 0.05$, ns: $p \geq 0.05$.

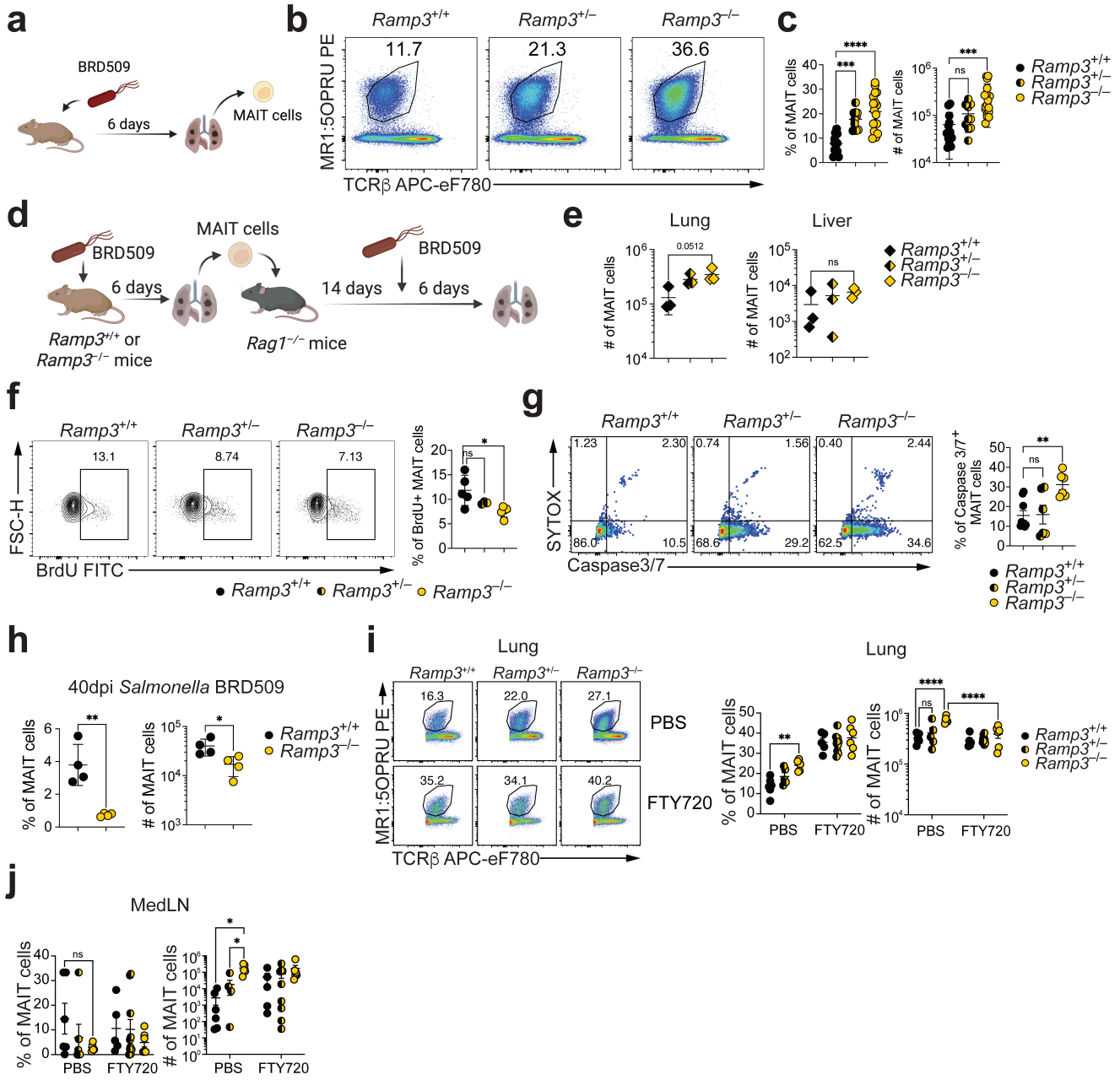


Figure 2

Increased MAIT cells in *Ramp3*$^{-/-}$ mice after bacterial infection.

a) Mice were inoculated with BRD509 *Salmonella enterica serovar Typhimurium* (BRD509) and analyzed 6 days after. **b)** Representative dot plots of lung MAIT cells 6 days after infection. **c)** Frequencies and absolute numbers of MAIT cells in the lung of *Ramp3*$^{-/-}$ mice and control mice 6 days after infection. n = 13;10;17 for wild-type, heterozygous and knockout, respectively. Results from multiple experiments. **d)** Schematic of adoptive transfer protocol for MAIT cells increased after bacterial infection. **e)** Accumulated data of *Ramp3*$^{-/-}$ and control MAIT cells present in the lungs and livers of *Rag1*$^{-/-}$

recipient mice. n = 3 for each group. **f)** BrdU incorporation and **g)** expression of apoptotic markers, SYTOX and Caspase3 by *Ramp3*$^{-/-}$ and control lung MAIT cells 6 days after infection. **h)** Percentage and absolute number of lung MAIT cells 40 days after infection. n = 5;3;5 for wild-type, heterozygous and knockout, respectively. **i)** Dot plot of MAIT cells in the lungs of *Ramp3*$^{-/-}$ mice 6 days after BRD509 infection when treated with FTY720 or controls and frequency and absolute count of *Ramp3*$^{-/-}$ lung or **j)** mediastinal lymph node (MedLN) MAIT cells after 6 days of BRD509 infection in mice treated with FTY720 or PBS control. Lung PBS n = 6;5;5 for wild-type, heterozygous and knockout, respectively; Lung FYT720 n = 5;10;6 wild-type, heterozygous and knockout, respectively. Lines indicate mean ± SE. Data analyzed by two-way ANOVA, one-way ANOVA with post-hoc Tukey or Krustal-Wallis with post-hoc Dunn's test. ****: $p < 0.0001$, ***: $p < 0.001$, **: $p < 0.01$, *: $p < 0.05$, ns: $p \geq 0.05$.

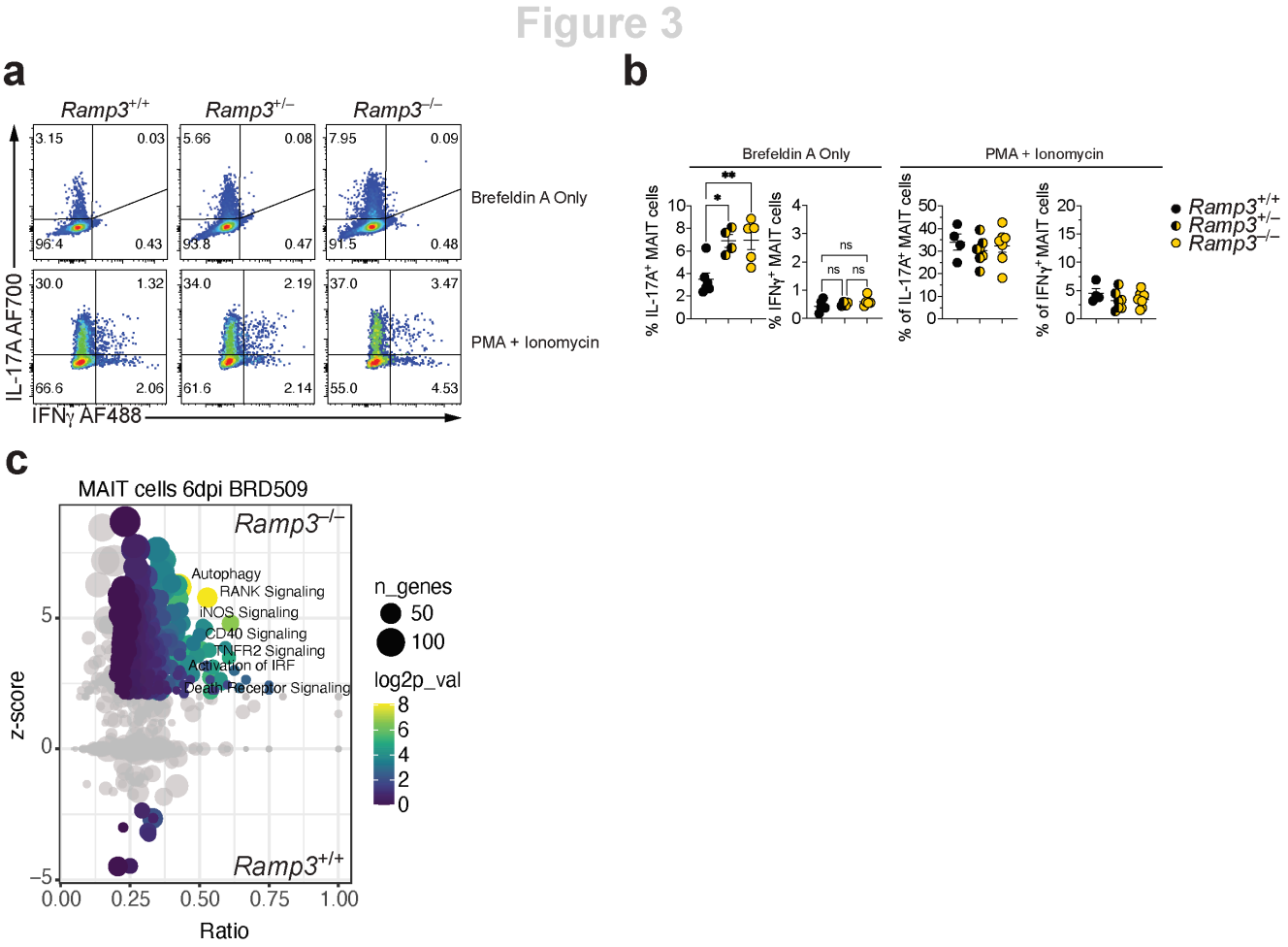


Figure 3

MAIT cells in *Ramp3*$^{-/-}$ mice have altered cytokine secretion

a) IL-17A and IFNg detected by intracellular flow cytometry in lung MAIT cells of *Ramp3*$^{-/-}$ and control mice after infection. Cells were either analyzed *ex vivo* treated with Brefeldin A or re-stimulated with PMA and Ionomycin. Brefeldin A: n = 6;4;5 for wild-type, heterozygous and knockout, respectively; PMA/Ionomycin: n = 4;7;7 for wild-type, heterozygous and knockout, respectively. **b)** Accumulated data of lung MAIT cell IL-17A and IFNg production. Lines indicate mean ± SE. Data analyzed by one-way ANOVA with post-hoc Tukey or Krustal-Wallis with post-hoc Dunn's test for multiple comparisons. **: $p < 0.01$, *: $p < 0.05$, ns: $p \geq 0.05$. **c)** Pathway analysis of transcriptomes of *Ramp3*$^{-/-}$ and control lung MAIT cells 6 days after infection.

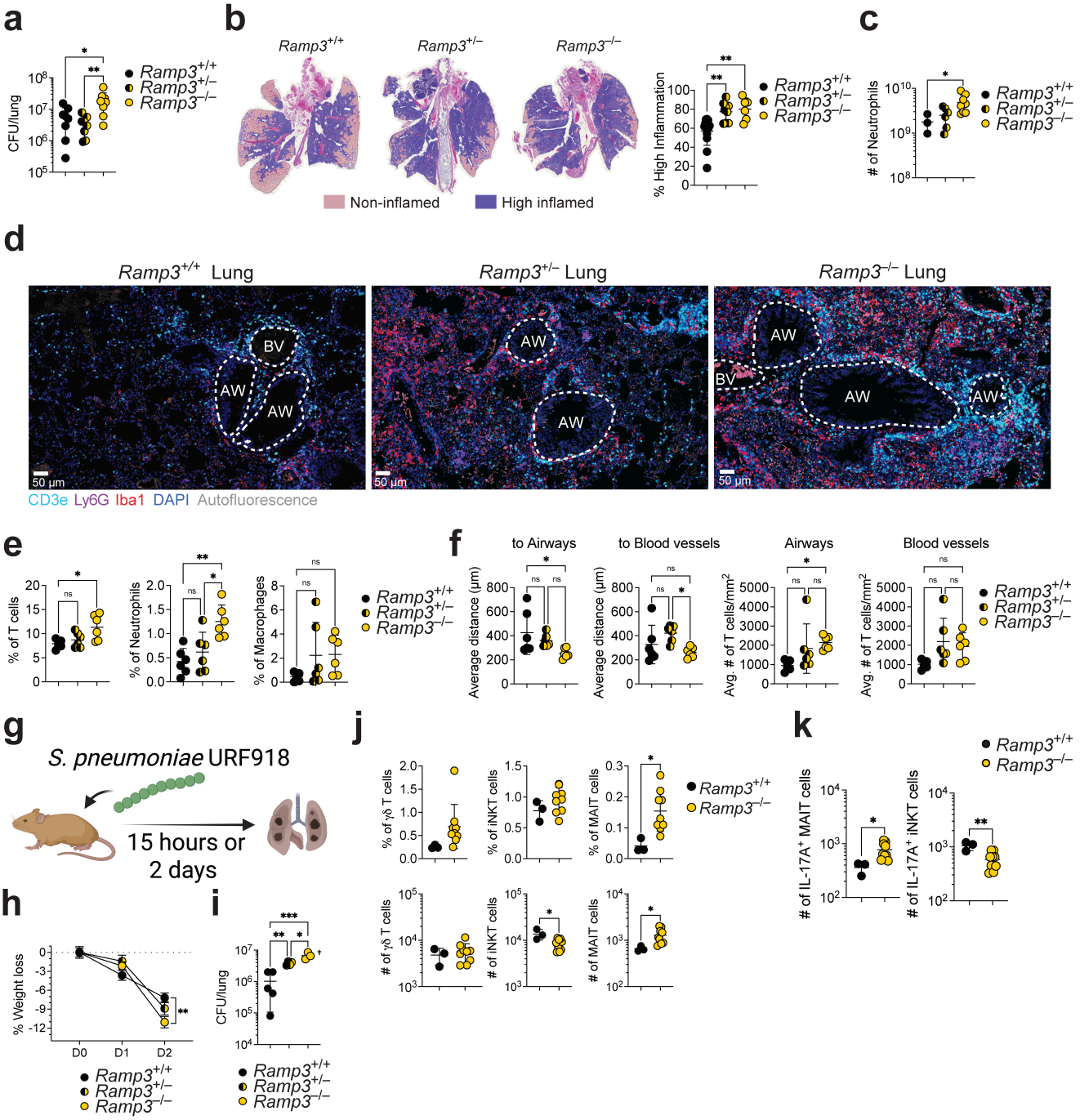


Figure 4

Tissue damage and differential distribution of immune cells in *Ramp3*$^{-/-}$ and control lungs after infection.

a) Lung bacterial burden 6 days after *Salmonella* BRD509 infection. n = 9;8;8 for wild-type, heterozygous and knockout, respectively. **b)** (*left*) Whole slide scan of lung sections stained with Hematoxylin and

Eosin and overlayed with a pixel classifier defined areas of high (*purple*) and low (*pink*) inflammation. (*right*) Proportion of the area of whole slide sections classified as high inflammation at day 6 after infection in wild-type, heterozygous, and *Ramp3*$^{-/-}$ mice. n = 13;9;6 for wild-type, heterozygous and knockout, respectively. **c)** Flow cytometry analysis of absolute numbers of lung neutrophils 6 days after infection. n = 3;6;8 for wild-type, heterozygous and knockout, respectively. **d)** Representative regions of interest (ROI) of immunofluorescent-stained sections of the whole lung. Tissue structures were annotated as AW: airway and BV: blood vessel. **e)** Frequencies of T cells, neutrophils and macrophages classified by staining of tissue sections with anti-CD3e, Ly6G and Iba1, respectively. Cell types were detected in immunofluorescent-stained whole lung slides by cell segmentation and classification in QuPath. n = 6;4;6 for wild-type, heterozygous and knockout, respectively. **f)** (*left*) Average distances of T cells to either airways or blood vessels. (*right*) Average number of T cells within 50 µm surrounding airways and blood vessels. n = 6 for each group. Lines indicate mean ± SE. Data analyzed by one-way ANOVA with post hoc Tukey or Krustal-Wallis with post-hoc Dunn's test for multiple comparisons. ***: $p < 0.001$, **: $p < 0.01$, *: $p < 0.05$, ns: $p \geq 0.05$. **g)** *Streptococcus pneumoniae* strain URF918 infection in *Ramp3*$^{-/-}$ and control mice. **h)** Weight loss in *Ramp3*$^{-/-}$ and control mice after *S. pneumoniae* infection. n = 5;4;4 for wild-type, heterozygous and knockout, respectively. **i)** Bacterial burden in mice lungs after 2 days of *S. pneumoniae* infection. n = 3;4;5 for wild-type, heterozygous and knockout, respectively. †: One *Ramp3*$^{-/-}$ mouse died at day 2 and was excluded from the analysis. **j)** Percentage and absolute number of innate-like T cells in the lungs of *S. pneumoniae* infected mice. **k)** Absolute number IL-17A^{+} MAIT cells and iNKT cells after 14 hours of *S. pneumoniae* infection. n = 3 for wildtype and n = 9 for knockout. Lines indicate mean ± SE. Data analyzed by unpaired two-tailed t-test. **: $p < 0.01$, *: $p < 0.05$, ns: $p \geq 0.05$.

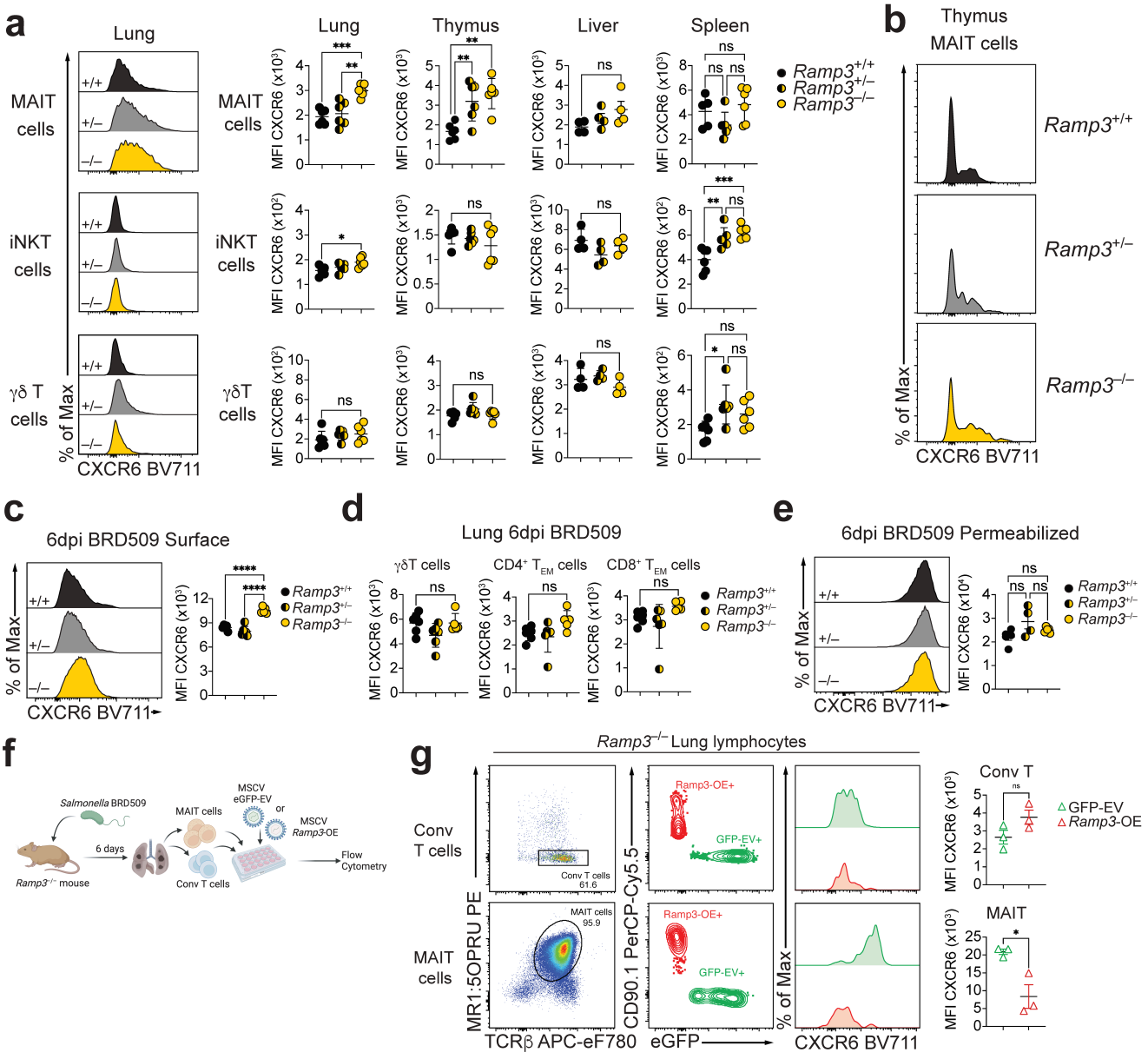


Figure 5

Increased CXCR6 in *Ramp3*$^{-/-}$ lung MAIT cells.

a) Surface expression of CXCR6 by *Ramp3*$^{-/-}$ and control strain MAIT cells from the indicated tissues at steady-state. n = 6 for each group. **b)** Surface expression of CXCR6 by thymic MAIT cells at steady-state. n = 6 for each group. **c)** Levels of CXCR6 by *Ramp3*$^{-/-}$ and control strain lung MAIT cells 6 days after infection. n = 5;6;5 for wild-type, heterozygous and knockout, respectively. **d)** Surface expression of CXCR6 on the indicated lung T cell subpopulations from infected *Ramp3*$^{-/-}$ and control mice. n = 6;6;5 for wild-type, heterozygous and knockout, respectively. **e)** Total CXCR6 stained on permeabilized lung

MAIT cells 6 days after infection of *Ramp3*$^{-/-}$ and control mice. n = 5;4;5 for wild-type, heterozygous and knockout, respectively. Lines indicate mean ± SE. Data analyzed by one-way ANOVA with post-hoc Tukey for multiple comparisons. ****: $p < 0.0001$, ***: $p < 0.001$, **: $p < 0.01$, *: $p < 0.05$, ns: $p \geq 0.05$. **f)** Illustration of the experimental scheme for RAMP3 overexpression. **g)** Dot plot on sorted conventional T cells and MAIT cells transduced with MSCV *Ramp3*-OE (red) and MSCV GFP-EV (green). Histogram of expression of CXCR6 on *Ramp3*-OE^{+} and GFP-EV^{+} cells and cumulated data plots. n = 3 per group. Data analyzed by Student's t-test. *: $p < 0.05$, ns: $p \geq 0.05$.

Figure 6

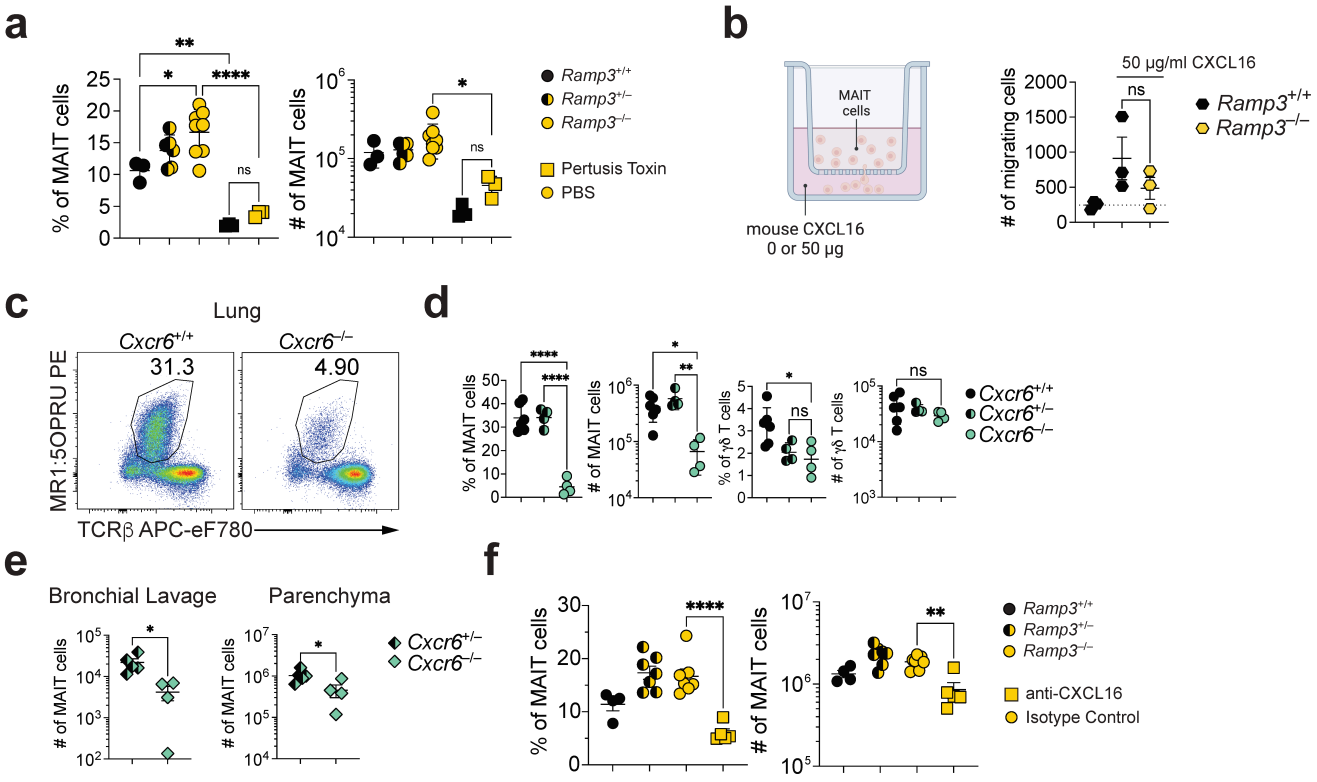


Figure 6

MAIT cell accumulation in infected lungs is dependent on CXCR6-CXCL16.

a) Frequency and absolute count of *Ramp3*$^{-/-}$ and control strain lung MAIT cells 6 days after infection in mice treated with Pertussis Toxin or PBS control. PBS n = 3;6;8 for wild-type, heterozygous and knockout, respectively; Pertussis Toxin n = 3 for each group. **b)** (*left*) Illustration of transwell migration experiments. BRD509-expanded lung MAIT cells were seeded in the top transwell and then placed into the bottom well with or without 50 µg of mouse recombinant CXCL16. Cells migrating to the lower chamber were then counted. (*right*) Accumulated data of migration assay with or without CXCL16. n = 3 per group. **c)** Dot plot of MAIT cells in *Cxcr6*$^{-/-}$ and control mice 6 days after infection. **d)** Accumulated flow cytometry data of frequencies and absolute numbers of lung MAIT and gd T cells in *Cxcr6*$^{-/-}$ and control mice 6

days after infection. n = 6;4;4 for wild-type, heterozygous and knockout, respectively. **e)** Absolute number of adoptively transferred *CXCR6*$^{+/-}$ or *CXCR6*$^{-/-}$ MAIT cells in the bronchiolar lavage and parenchyma of *Rag1*$^{-/-}$ mice 6 days after infection. n = 5 and 4 for heterozygous and knockout, respectively. **f)** Frequency and absolute count of *Ramp3*$^{-/-}$ and control lung MAIT cells 6 days after infection of mice injected with anti-mouse CXCL16 or isotype control antibody. IgG1 isotype n = 4;7;7 for wild-type, heterozygous and knockout, respectively; anti-CXCL16 n = 5. Lines indicate mean ± SE. Data analyzed by one-way ANOVA with post-hoc Tukey for multiple comparisons or unpaired t-test. ****: $p < 0.0001$, ***: $p < 0.001$, **: $p < 0.01$, *: $p < 0.05$, ns: $p \geq 0.05$.

Supplementary Files

This is a list of supplementary files associated with this preprint. Click to download.

- suppltable1DEG00.xlsx
- suppltable2DEG06.xlsx
- suppltable3canonical.xlsx
- suppltable4upstream.xlsx
- suppltable5reagents.xlsx
- figS1copy.pdf
- figS2copy.pdf
- figS3copy.pdf
- figS4copy.pdf
- figS5copy.pdf